Available online at www.sciencedirect.com

ScienceDirect

Energy Procedia 45 (2014) 759 – 768

Energy Procedia

68th Conference of the Italian Thermal Machines Engineering Association, ATI2013

CFD analysis of the acoustic behavior of a centrifugal compressor for high performance engine application

Stefano Fontanesi[a]*, Stefano Paltrinieri[a], Giuseppe Cantore[a]

[a]*Department of Engineering "Enzo Ferrari", University of Modena and Reggio Emilia, Modena, Italy*

Abstract

The paper reports an activity aiming at the characterization of the acoustic noise of a centrifugal compressor for a currently made high performance engine. All the analyses are carried out through the use of Detached Eddy Simulation. During high-load / low-engine speed operations of the engine, the compressor exhibits noise peaks above 150 dBA at relatively low frequencies, whose origin is relatively hard to rationalize. The use of three-dimensional CFD simulation appears to be very promising to gain a better understanding of the complex flow structures at the compressor inlet as well as to promote design optimizations aiming at limiting the acoustic emissivity of the component. In view of the dependency of the acoustic phenomena on the instantaneous pressure waves and flow structures, fully transient CFD simulations are highly recommended, together with the use of sophisticated numerical techniques such as Large Eddy and Detached Eddy simulation [1], [2], which are widely recognized to be able to better capture highly unstable features than the common RANS approach [3], [4]. In order to limit the computational cost of the analyses, preliminary steady-state RANS simulations are carried out to both initialize the flow field and to evaluate the grid capability to properly match the desired frequency spectrum.

"Keywords: DES, centrifugal compressor, acoustic, noise"

1. Introduction

In the last few years, gasoline engines are retrieving market shares against Diesel units. This is mainly due to the increasing pollutant emission restrictions and to the development of a new generation of highly downsized, direct injected units capable of combining a high fuel conversion efficiency and an excellent drivability with limited tailpipe emission levels. In order to increase the specific power output, last generation of gasoline engines is

* Corresponding author. Tel.: +39-059-2056114; fax: +39-059-2056126.
E-mail address: stefano.fontanesi@unimore.it

doi:10.1016/j.egypro.2014.01.081

commonly coupled with either a supercharging or a turbocharging system, both of which are able to provide up to 50% increase in brake specific mean effective pressure levels at high engine loads in comparison with naturally aspirated units, while allowing non-negligible fuel consumption savings at low engine loads [5], [6].

In order to maximize the benefits deriving from turbocharging and downsizing, the choice of the proper turbocharger and its optimal matching with the engine is mandatory. For very low engine speeds, turbocharged engines may exhibit less torque and slower transient response than naturally aspirated engines. For the highest speeds, the turbine inlet temperature limits the maximum power of the engine and requires enrichment of the in-cylinder charge. Furthermore, the turbocharger may originate additional noise during some critical engine operations. The compressor analyzed in the paper is part of a turbocharger compound system designed for sport car applications, with and integrated compressor by-pass valve (CBV) system to avoid fluid hammer effects during throttled operations of the engine. During engine tests, the CBV was identified as a source of a disturbing noise peak of over 150dBA at relatively low frequency, whose origin was difficult to rationalize. In fact, the noise emission was experienced only during closed CBV operations of the turbocharger, in which the CBV admission pipe, located on a side of the compressor inlet, was acting as a Helmholtz's resonator, probably due to increased importance of the shear-layer excitation. The detailed experimental investigation of the compressor noise origin is far beyond the standard industrial practice, due to the complexity of the involved phenomena and to the need of advanced experimental techniques usually available only at highly specialized research laboratories. In this scenario, CFD can largely contribute to increase the understanding of the phenomenon due to the possibility to provide an extremely wide set of data, which are difficult to measure, with reasonable times and costs.

Due to the increasing computer power, in fact, it is nowadays possible to use refined numerical techniques such as large eddy simulation (LES) or detached eddy simulation (DES) to investigate complex problems of engineering interest [3], [4], [7]. Particularly, in this paper, DES simulation is chosen to investigate the compressor noise origin. The aim of the activity is twofold: on one side, experimental evidence of the noise emission is placed side by side to CFD simulations and used to evaluate the predictive capability of the numerical approach; on the other side, CFD is used to provide additional information and explanation of the noise source and eventually suggest possible design modifications. The computational domain is composed by the sole compressor system, and two different compressor operations are investigated, both characterized by the CBV in its closed position and the same rotational speed of 100.000 rpm, but with different levels of mass flow rate at the compressor inlet. The two operations exhibit opposite conditions in terms of noise source: particularly, one of the two is the one characterized by the above mentioned low-frequency / high-amplitude noise emission.

Prior to DES simulations, RANS steady flow analyses are performed in order to provide a preliminary forecast whether the designed computational grid is suitable to predict the noise source, in both position and amplitude. Furthermore, steady flow analyses are used to generate initial conditions, thus reducing the overall computational time of the subsequent DES unsteady simulations. In order to well-capture the measured frequency, transient analyses are then performed since noise emission is thought to be strictly correlated to the transient gasdynamic behavior of the CBV channel. All the simulations are performed using the commercial code Star-ccm+ licensed by CD-adapco [8], which is integrated with user routines and procedures. The proposed methodology is considered both a valid support to the experimental practice to deepen the understanding of the evidenced phenomena and a possible alternative during the early design stage, when the CBV geometry and its location should be chosen properly in order to avoid the unwanted screeching noise.

2. Experimental measurements and CFD domain construction

The experimental setup consists of basically two microphones near the right turbocharger, one triaxial accelerometer on the right compressor and one dynamic pressure sensor at the volute end, as illustrated in Figure1.

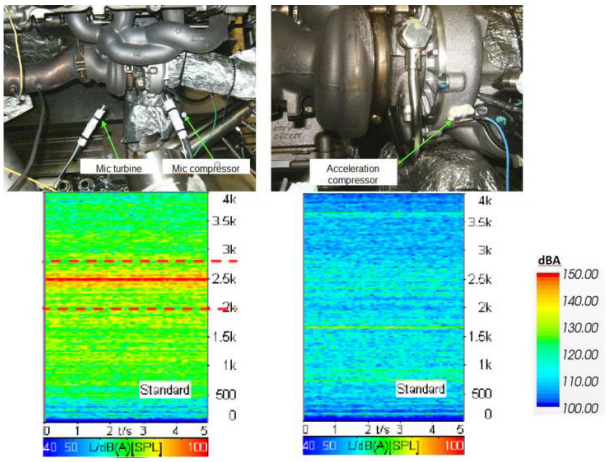

Fig. 1. Experimental apparatus and results.

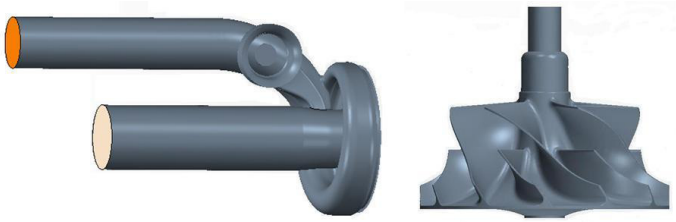

Fig. 2. Computational domain with extruded pipes and impeller geometry.

As stated in the introduction, different engine speeds and CBV positions were experimentally analyzed in order to evaluate the acoustic performance of the turbocharger and the onset of possible whistle noise. Details on either engine speeds and CBV positions cannot be reported explicitly for confidential reasons. As reported in Figure 1, the striking operating point exhibits a noise peak at about 2.5k Hz, whereas under non-striking conditions, the noise peak is much less pronounced. As stated earlier, the investigated compressor has an integrated CBV, which is located at the side-branch of the inlet pipe close to the 12 blade impeller. In turn, the membrane inside the pop-off valve has an asymmetric configuration. The simulations aim at reproducing the experimental evidence focusing on two different compressor operations, one striking and one non-striking; the geometrical domain, provided by the car manufacturer, is slightly different from the actual experimental layout. Particularly, as highlighted in Figure 2, both inlet and outlet pipes are straight and artificially extruded to allow the imposition of uniform and constant values. According to the available data, mass flow rate is imposed at the inlet position and pressure at the outlet, as reported in Table 1 for both the striking and the non-striking operations.

	Impeller Rotation Speed [rpm]	**Inlet Mass Flow Rate [kg/s]**	**Outlet pressure [Pa]**
Striking	100,000	0.0502	70,000
Non-striking	100,000	0.1205	60,000

Table 1. Compressor operating conditions.

In order to promote the calculation stability, inlet and outlet pipes are extruded of about 3 diameters to strengthen the assumption of uniform and constant conditions.

To capture the complex fluid/wall interaction, eleven wall layers are adopted with a first wall layer thickness which is capable to guarantee a y+ value close to unity in the impeller and CBV regions, as Figure 3 shows. Locally refined polyhedral cells are used with an overall cell count of about 9.6 million cells. The mesh size is locally decreased down to 0.6 mm over the whole CBV region, its junction with the inlet pipe and the impeller, as shown in Figure 4.

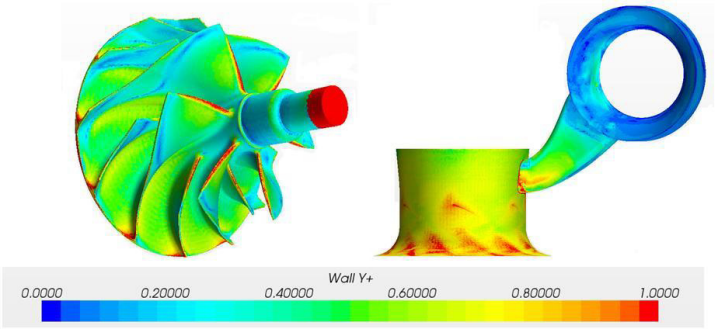

Fig. 3. Wall y^+ distribution.

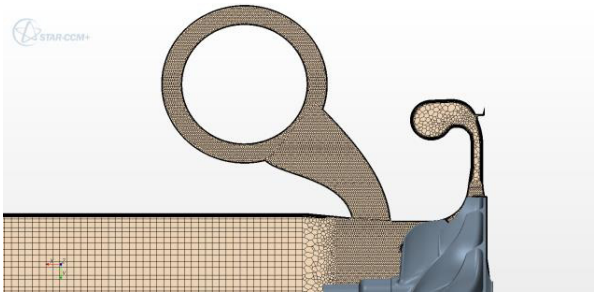

Fig. 4. Computational grid: detail of the refined mesh region.

3. Methodology

In order to get a first foresight of the compressor behavior, the CFD problem is preliminarily analyzed through a relatively simplified approach, i.e. steady-state RANS simulations of both compressor operating points. The impeller rotation is reproduced by the MRF (Moving Reference Frame) method which is based on the assumptions of constant angular velocity and static mesh [8]. Substantially, the grid flux is artificially calculated based on the properties of the reference frame rather than the local motion of cell vertices, the big advantage being that the mesh is generated only once.

The K-Ω-SST turbulence model formulation is chosen amongst the available ones for its well-known capabilities since it is able to restitute an accurate solution for typically detaching / re-attaching and swirling/rotating situations thanks to its accurate representation of the boundary layer [9], [10], [11].

Firstly, the striking condition is considered: the accuracy of the model is verified through the comparison between the predicted and measured pressure raise within the compressor. A preliminary qualitative aeroacoustic analysis is introduced in the steady-state calculations in order to qualitatively evaluate both the correctness of the mesh size and the emitted screech noise. The former is done by means of the “Mesh Frequency Cutoff” concept which is expressed by a scalar quantity representing the maximum solvable frequency for the given mesh size, according to equation 1. As visible, it depends on the local turbulent kinetic energy (k); provided the mean flow features are well captured by the adopted grid and model combination, an almost grid independent k field is reached, and the mesh frequency cutoff becomes inversely proportional to the local grid characteristic size:

$$f_{MC} = \frac{\sqrt{\frac{2}{3}k}}{2\Delta} \quad (1)$$

The latter is carried out through the so-called Proudman noise source model [12], which evaluates acoustic power per unit volume to determine the local contribution due to the turbulent flow. This model is typically used for RANS simulations and steady state solutions. The Proudman magnitude represents the local acoustic power generated by unit volume of isotropic turbulence having no mean flow [8] is represented by:

$$AP = \alpha\rho_0 \frac{u^3}{l}\frac{u^5}{a_0^5} \quad (2)$$

$$AP(dB) = 10log\left(\frac{AP}{p_{ref}}\right) \quad (3)$$

where α is coefficient related to the shape of the longitudinal velocity correlation, u is the root mean square of one of the velocity component, l is longitudinal integral length scale.

The steady-state solution is considered as convergent when the outlet section mass flow is contained within a given tolerance (less than 2%), for more than 200 samples, and of course equal to the inlet one. A non-negligible benefit from the steady-state solution is also that it provides consistent initial conditions for the subsequent transient analysis, and hence allows to limit the number of equivalent initial impeller rotations to be excluded before evaluating the acoustic analysis through the FFT analysis.

DES turbulence formulation is subsequently adopted to calculate the transient analysis, the main reason being that DES is not as demanding as pure LES formulation and resulting computational time decrement is a significant factor to take into account within industrial procedures. In DES, solid boundaries and locations where the turbulent length scale is smaller than the computational grid are modeled with a RANS approach, whereas LES is used everywhere the turbulent length scale exceeds the grid length. It is possible to state that most of the wall layer, which represents the most time consuming region because of the huge cell population, is therefore solved by the K-Ω-SST turbulence model [13], [14], [15]. The same approach is used for both operating conditions, striking and non-striking. Only boundary conditions are changed accordingly. Both transient analyses use an equivalent time step corresponding to a half degree impeller rotation, which provides an Average Convective Courant Number of about 0,3 and a maximum value of about 4 in a few cells, located right at the orifice between the compressor case and the impeller. Many probes, as reported in Figure 5, are located upstream the impeller and into the CBV to monitor pressure fluctuations. These pressure signals are recorded and then analyzed by means of Fast Fourier analysis and dBA power spectra in order to have a consistent comparison with the experimental measurements, especially to get the discretized frequency occurrence to be compared with measured data.

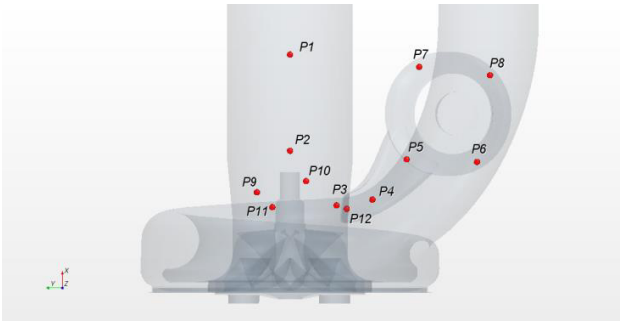

Fig. 5. Probe sensor locations.

4. results

4.1 Preliminary RANS analyses

The pressure raise across the compressor is at first checked, in order to evaluate the accuracy of the solution. A comparison is therefore carried out with the compressor characteristic curve, provided by the supplier. Surface averaged inlet pressure is monitored together with the outlet mass flow rate, this last just to evaluate the achievement of a perfectly steady solution.

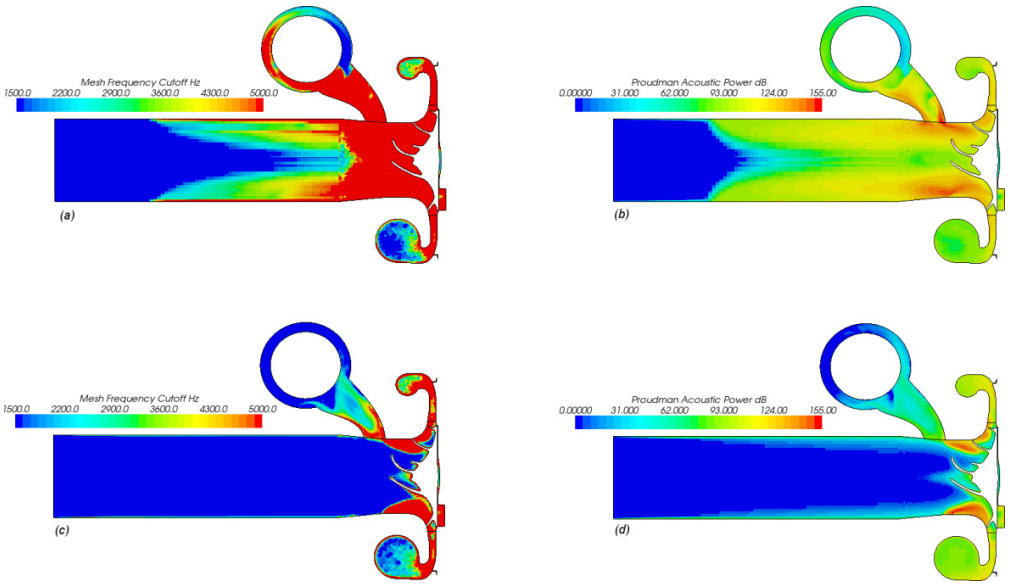

Fig. 6. Striking: (a)Mesh Frequency CutOff; (b) Proudman Acoustic Power. Non-striking: (c)Mesh Frequency CutOff; (d) Proudman Acoustic Power.

The resulting pressure raise for the striking condition is 67104 Pa, while for the non-striking one it increases up to 107354 Pa. This means that the preliminary simulation errors range between 4.1% and 5.0%.

Since the steady-state solutions are simply used to assess the grid suitability and to initialize the transient analysis, the results appear to be sufficiently accurate.

As shown in Figure 6 (a, c), where a section crossing the inlet channel and the CBV profile is reported, the f_{MC} is well above the experimental peak frequency, i.e. about 2.5 kHz.

As stated above, by means of the Mesh Frequency CutOff parameter it is possible to evaluate the mesh design suitability with reference to the expected frequency spectrum of the analyzed problem; particularly, the parameter evaluates whether the mesh is fine enough or if it needs some local refinements before computing the transient solution.

The observation of Figure 6 (a, c) confirms that the mesh size is more than adequate to capture frequencies up to the aforementioned one, particularly for the non-striking condition. For the non-striking one, a slight mesh refinement might be recommendable within the CBV region and at the CBV / inlet pipe junction, to try to counterbalance the reduced turbulent characteristics of the flow field.

The aeroacoustic model provides the noise source intensity in terms of detected dB, as highlighted by the Proudman Acoustic Power dB represented in Figure 6 (b, d); unfortunately, it does not reveal the corresponding frequency. To have access to this further information, a transient analysis has to be performed.

Observing Figure 6 (b), it is possible to see that the noise source for the non-striking condition is mainly located at the entrance of the CBV. In this region, a strong flow recirculation is detected even by the simplified RANS simulation. At the same time, results visible in Figure 6 (d) show that the Proudman acoustic distribution is

significantly decreased in the non-striking compressor operation, particularly in the compressor inlet pipe and in the proximity of the side-branch junction. This is due to the lack of the recirculation phenomenon visible in the striking case. Comparing Figure 6 (b, d), the Proudman Acoustic Power immediately restitute the noise decrement for the non-striking operation. In fact, orange to yellow spots are limited to a small portion close to the impeller zone.

4.2 Striking condition

As stated earlier, such preliminary simple steady-state simulations are mainly used to obtain reliable initial conditions for the subsequent transient analyses, in order to limit the impact of initial conditions on the establishment of a proper solution and to avoid the need to disregard too many equivalent impeller rotations at the beginning of the DES solution. For the specific investigations, 10 initial equivalent impeller rotations are discarded in order to evaluate the Fourier Transform signal.

Results of the striking condition are reported in Figure 7 and 8. The two pictures summarize the probe signals throughout the simulation time. As visible, signals need some time before developing into periodic fluctuations. This justifies the choice by the authors to arbitrarily discard the first ten equivalent impeller rotations, i.e. a corresponding time of 0.006 s.

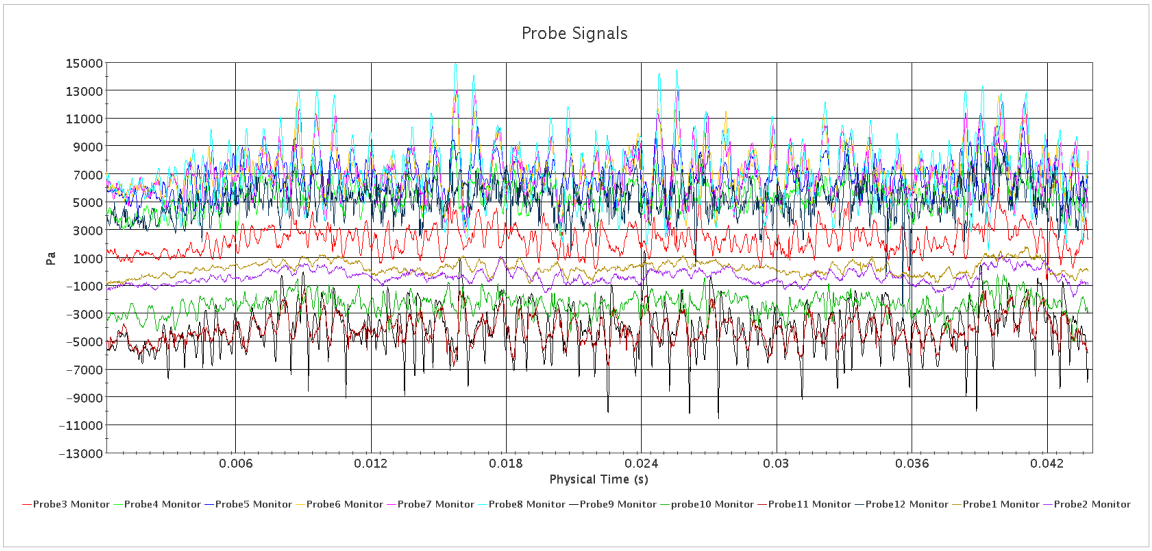

Fig. 7. Pressure fluctuations at the probe locations.

The overall simulation of the striking condition covers 73 equivalent impeller rotations on 64 cores; roughly 2 equivalent impeller rotations per day are computed. The signals are then analyzed by means of the A-Weighted Sound Pressure Level function, in order to have a fair comparison with the experimental measurements reported in Figures 1 (c) and (d).

The comparison between the experimental and numerical FFTs allow to state that the frequency of peak noise occurrence is well captured. Besides the maximum peak noise at about 2.5kHz, other relevant frequencies are also well represented. In fact, the experimental FFT signal reveals that relevant noise increments are visible within the 1kHz to 1.5kHz range, as well as at 1.75kHz. These additional noise peaks are again found to be in fairly good agreement with the CFD simulation. The comparison with experimental measurements shows that the adopted approach is a valid contribution, and even a possible alternative, to the experimental investigation, demonstrating that CFD can be a reliable tool to discern among different geometrical configurations at the design stage.

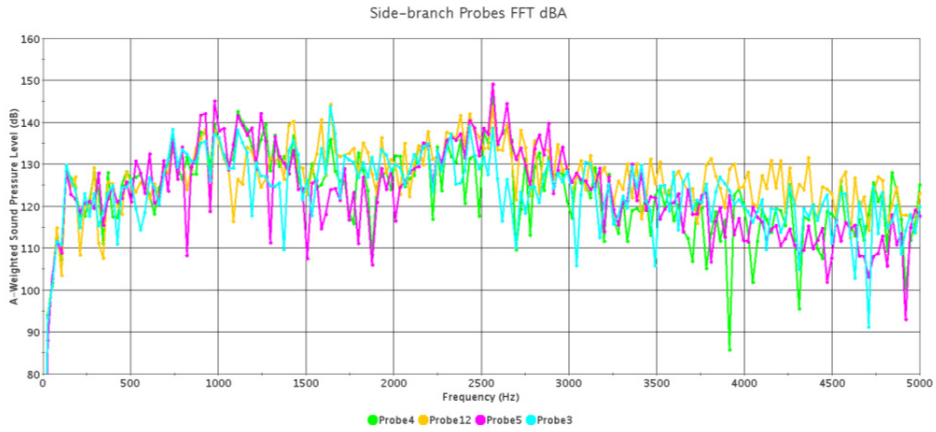

Fig. 8. Side-branch FFT signals, the maximum peak occurs close to 2.5 kHz.

4.3 Non-striking condition

The same modeling strategy is adopted for the second operating point. In fact, although results from the preliminary RANS simulations clearly highlight that the second investigated operation is characterized by a better acoustic behavior than the previous one, a transient DES analysis is again carried out.

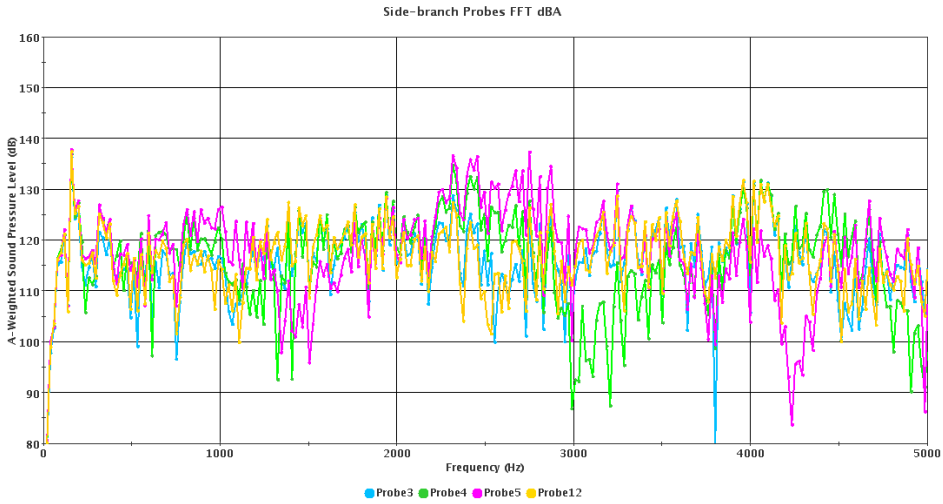

Fig. 9. Non-striking FFT of the side-branch probe signals.

Despite the reduced criticality of the new compressor operation, the same number of equivalent impeller rotations is analyzed.

Results seem once again to be consistent with the experimental evidence. They are summarized in Figure 9.

It can be recognized that the noise peak at about 2.5 kHz is relevantly decreased in comparison with the striking operating condition. The spectrum is now more homogeneous, and low-frequency peaks appear around 250 Hz. This confirms, as anticipated from the RANS results, that the non-striking condition has a better acoustic behavior since the inlet flow field is highly structured close to the impeller region and the recirculation zone is limited. The acoustic behavior is reasonably captured in terms of both amplitude and frequency, despite the numerical forecast is now less adherent to the experimental evidence. Some slight differences in both peak amplitude and position can in fact be

noticed between the CFD simulation and experimental results. The reason can be twofold. Firstly, the required simulated time might be longer than for the striking case to provide a detailed reconstruction of the wide frequency spectrum. Secondly, as previously showed in the RANS section, this operating condition exhibits an optimal Mesh Frequency CutOff region which is strictly limited to the side-branch inlet; this suggests that the cell size should be slightly decreased in order to better capture frequencies above 1.5 kHz / 2kHz in the remaining part of the CBV ring and close to the impeller region.

However, in terms of qualitative comparison with the striking condition, the problem is addressed at the side-branch inlet, where the Mesh Frequency CutOff requirement is fulfilled, and it is possible to state that the non-striking operation does not produce the same whistle noise amplitude as that detected for the striking one.

5. Conclusions

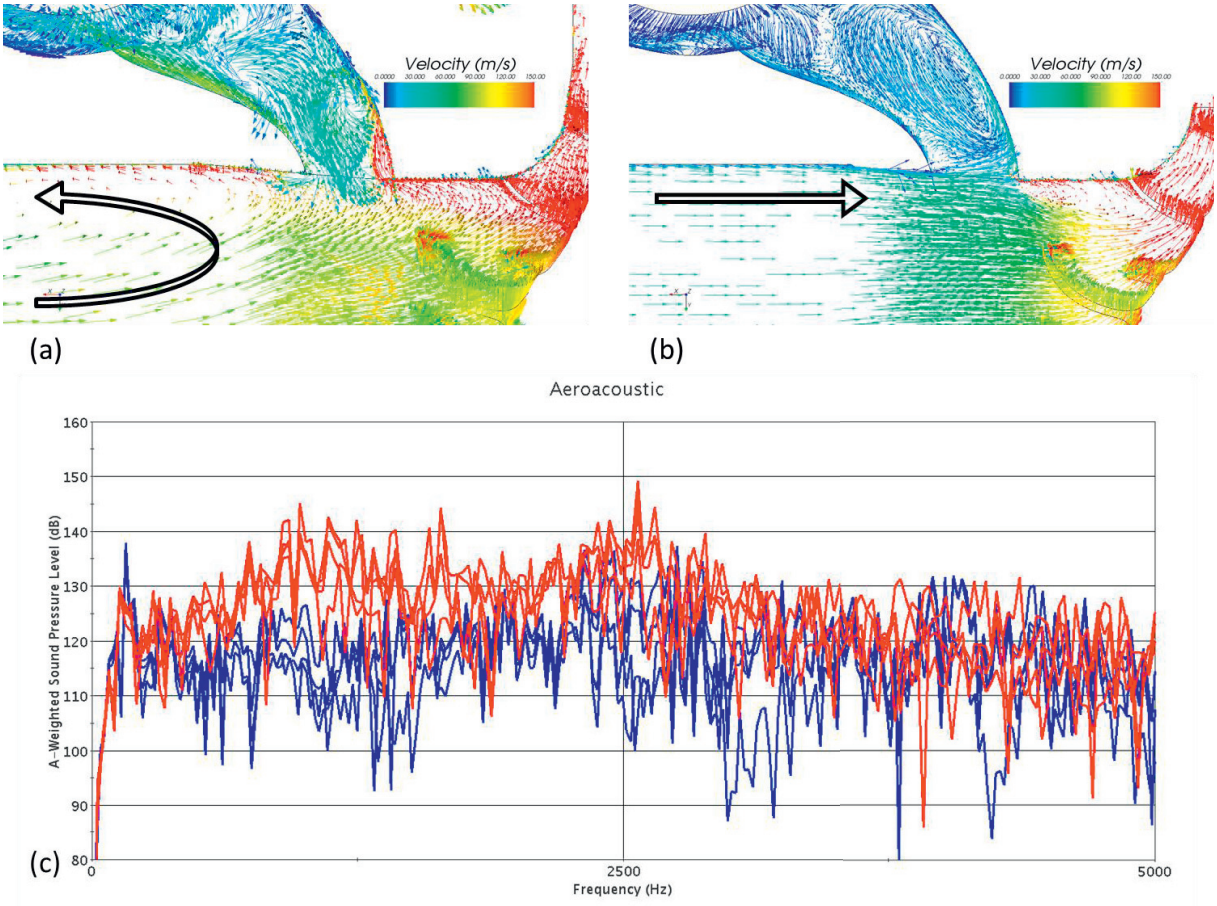

Fig. 10. Velocity field distribution (a, b) and FFT comparison between the two operating conditions (c).

In this paper, the acoustic behavior of a centrifugal compressor is investigated in order to provide potential explanations for the experimentally detected acoustic noise experienced during some engine tests. In order to fulfill this purpose, two different operating conditions are analyzed by means of both steady RANS and unsteady DES simulations. RANS simulations are preliminarily used to provide both a qualitative evaluation of the designed computational grid and consistent initial conditions for the subsequent transient analyses. DES simulations demonstrate to be able to discern the striking operating condition from the non-striking one. This is further highlighted in Figure 10, where a direct comparison between the two compressor operations is reported in terms of

both flow patterns on a plane section cutting the side-branch and of emitted noise spectra. The strong pulsating flow at the compressor inlet, promoting a periodic flow detachment and re-attachment at the CBV junction, is found to be the major cause of the experimental whistle under the striking operating condition, which is very close to the surge limit of the compressor. Figure 10 (a) highlights the wide recirculation zone upstream the CBV and the secondary one at the CBV / impeller junction. Conversely, under the non-striking condition the flow field within the inlet pipe is well aligned and more structured; consequently, eddies are both less pronounced and less likely to span the pop-off valve, hence promoting acoustic fluctuations. The implemented methodology proves to be able to address the critical frequencies in the striking case; for the non-striking one, probably, a wider set of equivalent impeller rotations and a slightly finer grid would be recommendable. Still, the emitted noise is consistent with the measured one for both conditions. The approach is reliable and can be adopted either in conjunction with the experimental investigations, to provide additional information and a deeper understanding of the involved phenomena, or as a preliminary design tool to evaluate possible solutions with limited time and resources. For the analyzed case, countermeasures to reduce the striking condition noise are under investigation. Among the possible solutions, the addition of a ported shroud close to the side-branch could be able to extend the operational range of the compressor by increasing the surge margin. The port shroud would help to limit the recirculation zone, thus improving the inlet flow field stability. Further study will be addressed to evaluate different grid construction techniques, as well as for BCs appliance, in order to further reduce computational times. In addition, new turbulence approaches, including fully LES ones, will be used in order to have a better estimation on the noise amplitude prediction.

References

[1] Tucker PG. Computation of unsteady turbomachinery flows: Part 1—Progress and challenges. Progress in Aerospace Sciences, Volume 47, Issue 7, October 2011, Pages 522-545, ISSN 0376-0421, http://dx.doi.org/10.1016/j.paerosci.2011.06.004

[2] Olausson M. Turbomachinery aeroacoustic calculations using non-linear methods. PhD Thesis, Department of Applied Mechanics, Chalmers University of Technology, Gothenburg, Sweden, 2011

[3] Fontanesi S, Paltrinieri S, d'Adamo A, Cantore G et al. Knock Tendency Prediction in a High Performance Engine Using LES and Tabulated Chemistry. SAE Int. J. Fuels Lubr. 6(1):98-118, 2013, doi:10.4271/2013-01-1082

[4] Fontanesi S, Paltrinieri S, d'Adamo A, Duranti S. Investigation of boundary condition and field distribution effects on the cycle-to-cycle variability of a turbocharged GDI engine using LES. Oil & Gas Sci. Tech., doi: 10.2516/ogst/2013142

[5] Lecointe B and Monnier G. Downsizing a Gasoline Engine Using Turbocharging with Direct Injection. SAE Technical Paper 2003-01-0542, 2003, doi:10.4271/2003-01-0542

[6] Cruff L, Kaiser M, Krause S, Harris R et al. EBDI® - Application of a Fully Flexible High BMEP Downsized Spark Ignited Engine. SAE Technical Paper 2010-01-0587, 2010, doi:10.4271/2010-01-0587

[7] Lee S, Kim H, Runchal A. Large eddy simulation of unsteady flows in turbomachinery. Proceedings of the Institution of Mechanical Engineers, Part A: Journal of Power and Energy 2004; 218(7): 463–75

[8] CD-adapco, STAR-CCM+ Version 7.06 User Guide, 2012

[9] Wilcox D. Turbulence modelling for CFD. DCW Industries Inc.; 1993

[10] Menter F. Zonal two equation k–l turbulence models for aerodynamic flows. Paper AIAA-93-2906; 1993

[11] Tucker P. Turbulence modelling for problem aerospace flows. International Journal for Numerical Methods in Fluids 2006; 51(3): 261–83

[12] Sarkar S, Hussaini MY. Computation of the Sound Generated by Isotropic Turbulence. NASA Report 191543, ICASE Report No. 93-74, 1993

[13] Michelassi V, Wissink J, Rodi W. Direct numerical simulation, large eddy simulation and unsteady Reynolds-averaged Navier Stokes simulations of periodic unsteady flow in a low-pressure turbine cascade: a comparison. Proceedings of the Institution of Mechanical Engineers, PartA: Journal of Power and Energy 2003; 217(4): 403–11

[14] Suzen Y, Huang P. Numerical simulation of unsteady wake / blade interactions inlow-pressure turbine flows using an intermittency transport equation. Journal of Turbomachinery 2005; 127: 431–44.

[15] Strelets M. Detached eddy simulation of massively separated flows. In: Proceedings of the AIAA, aerospace sciences meeting and exhibit,39th Reno, NV; 2001, AIAA Paper2001-0879.